

Absence of a Superradiant Phase Transition in Dirac Landau Polaritons

Elsa Jöchl,^{1,2} Felix Helmrich,^{1,2} Frieder Lindel,^{2,3} Lucy Hale,^{1,2} Lorenzo Graziotto,^{1,2}
Mona Jarrahi,⁴ Tobia F. Nova,⁵ Jérôme Faist,^{1,2} and Giacomo Scalari^{1,2}

¹*Institute for Quantum Electronics, ETH Zürich, Zürich 8093, Switzerland*

²*Quantum Center, ETH Zürich, Zürich 8093, Switzerland*

³*Institute for Theoretical Physics, ETH Zürich, Zürich 8093, Switzerland*

⁴*Terahertz Electronics Laboratory, UCLA, Los Angeles 90095, United States*

⁵*Department of Quantum Matter Physics, University of Geneva, Geneva 1211, Switzerland*

(Dated: May 27, 2026)

The condensation of photons into a macroscopically populated ground state, a superradiant phase transition (SRPT), is one of the most striking predictions of cavity quantum electrodynamics (cQED) [1, 2], yet has resisted experimental realization in equilibrium for over fifty years. Whether such a transition can survive at all in light-matter coupled systems is still debated, with a widely established *No-Go* theorem ruling it out across several models [3–5]. Graphene cyclotron transitions ultrastrongly coupled to terahertz (THz) cavities have been at the heart of this debate [6, 7]. At leading order, the linear Dirac dispersion of electrons does not generate the diamagnetic \vec{A}^2 term that enforces the theorem, making graphene the cleanest candidate for a No-Go-evading phase transition.

Here, we present the first THz spectroscopic measurements of an encapsulated monolayer graphene flake ultrastrongly coupled to a single complementary split-ring resonator. By tuning the carrier density we sweep the system from weak coupling into the ultrastrong regime, reaching a normalized coupling $\Omega_R/\omega_{\text{cav}} \approx 0.4$. This is well into the range where a second order SRPT would manifest by a softening of the lower polariton branch, which we do not observe. The full polariton dispersion is instead quantitatively reproduced by a Hopfield Hamiltonian derived from first principles using a near-field model that accounts for the sub-wavelength character of the cavity.

Our results establish an experimental baseline for predictions of cavity-driven phase transitions in two-dimensional Dirac systems, and rule out a No-Go-evading SRPT in graphene Landau polaritons up to the strongest couplings accessible today, with direct implications for proposals invoking vacuum-induced order in solid-state cQED.

INTRODUCTION

The term superradiance was first introduced by R.H. Dicke to explain the coherent emission of light by N two-level atoms placed in the same electromagnetic environment [8]. If the two-level systems are placed at distances a fraction of the electromagnetic wavelength and display identical coupling to the photon field [9], both the emission amplitude and decay rate will scale with N , giving rise to a superradiant intensity burst proportional to N^2 . This finding, based on the Dicke Hamiltonian, made way for Hepp and Lieb to propose criticality in the ground-state of a cavity mode interacting with an ensemble of atoms in the thermodynamic limit [1]. Shortly thereafter also studied in a paper by Hioe and Wang, the superradiant phase transition (SRPT) would become a long sought-after experimental challenge [2].

A SRPT is a continuous phase transition, characterized by the buildup of a macroscopically populated, coherent photonic ground state above a critical coupling strength η_c [1, 2, 10, 11]. Spectrally, this translates to a softening of the lower polariton branch of the coupled system, as shown in Figure 1a. Various dissipative-driven systems (such as thermal atomic vapors and Bose-Einstein condensates) have since been experimentally shown to exhibit non-equilibrium SRPTs, with external pumping necessary to induce the phase transition [12–14]. In the

last 15 years, special attention has been devoted to solid-state and semiconductor systems [15], where the presence of large carrier densities and subwavelength cavities allows the exploration of ultrastrong light-matter coupling regimes. While an equilibrium magnon-spin SRPT-analogue has been reported in [16], the experimental realization of a photonic equilibrium SRPT remains elusive.

The occurrence of second-order SRPTs in cavity quantum electrodynamic (cQED) systems has been disputed with the postulation of the so-called *No-Go theorem* [3–5]. Allowing for the criticality of the Dicke Hamiltonian is the truncation of interaction terms $\mathcal{O}(\vec{A}^2)$ (with the electromagnetic vector potential \vec{A}). However, with higher coupling strengths this truncation is no longer a valid approximation. The diamagnetic contribution (given by the \vec{A}^2 -term) of the strongly interacting electric field needs to be accounted for, ensuring the preservation of the f-sum rule, as well as gauge invariance [3–5, 17–19]. The inclusion of this term exactly counteracts the emergence of the SRPT, and leads to the well known Hopfield Hamiltonian which has been shown to accurately describe ultrastrongly coupled light-matter systems [20–22]. An exception is constituted by Landau polaritons in non-parabolic SiGe quantum wells where a LP softening has been observed [23].

Still in search of a novel phase transition, this has inspired many theoretical predictions and counter-

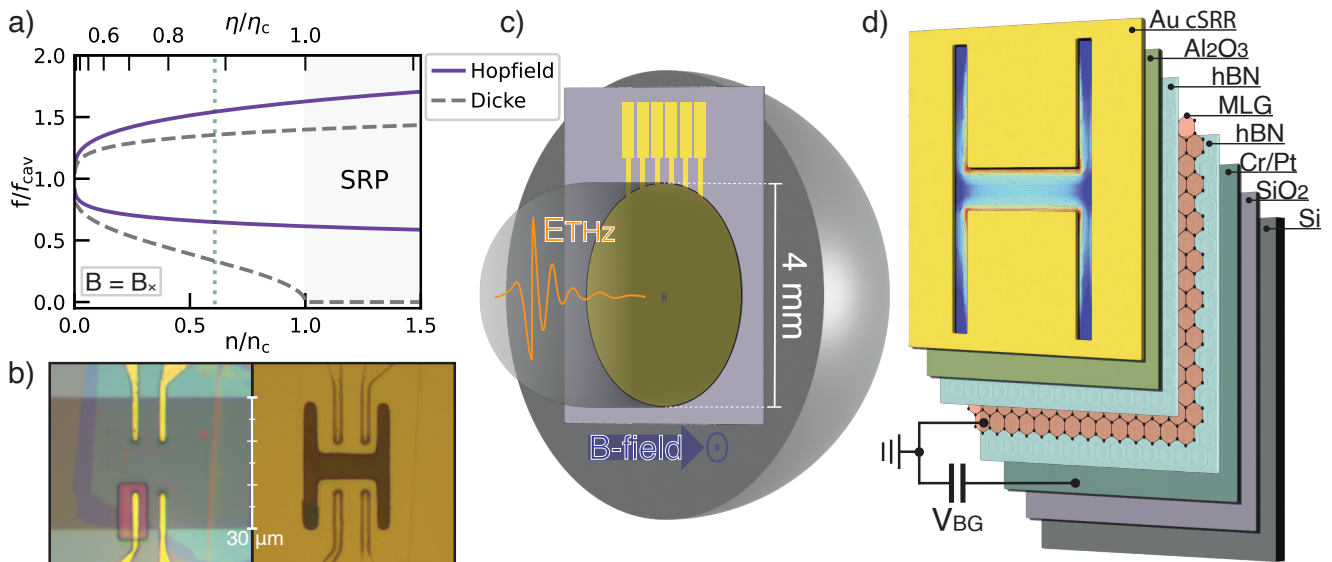


FIG. 1. **Probing SRPTs in monolayer graphene.** **a)** Dispersion of the lower and upper polariton branches as a function of density n (coupling η) at resonance in the Dicke (grey dashed lines) and Hopfield models (purple lines). While the Dicke prediction exhibits criticality with softening to zero frequency of the lower branch, the Hopfield model does not. The density range where a superradiant phase (SRP) is predicted in the Dicke model is indicated by the grey background. **b)** Top view of the sample before (left) and after (right) the deposition of the cSRR. **c)** Schematic view of the experimental setup. The sample consisting of the graphene flake and the cSRR is mounted between silicon immersion lenses. A linearly polarized THz pulse E_{THz} (orange) is incident on the sample. A static magnetic field (purple) orthogonal to the graphene plane quantizes the electron motion in graphene to Landau levels. **d)** Precise stack-up of the sample. The graphene flake is encapsulated by hBN flakes and connected electrically using etch contacts. A thin metallic Cr/Pt layer acts as an electrostatic gate by applying a static voltage V_{BG} with respect to graphene. The cSRR is fabricated from Au on top of the graphene heterostructure and is electrically insulated from the latter using alumina (Al_2O_3) dielectric. The distribution of the in-plane electric field obtained by finite-element simulations. The substrate consists of Si with a 285 nm oxide layer.

arguments about systems in which the *No-Go theorem* could be circumvented [17, 24–28]. The ultrastrong interaction of graphene cyclotron transitions with a Terahertz (THz) cavity mode became a platform of discussion for exactly such a debate [6, 7]. Owing to the linear dispersion of graphene carriers, the diamagnetic term does not arise directly in a minimal coupling approach [6], but is only generated when considering interband transitions [7].

To investigate the behavior of such graphene Landau polaritons in the ultrastrongly coupled regime, THz transmission spectroscopy has to be performed under the influence of a magnetic field. While far field spectroscopy of large-scale graphene flakes can be performed in the THz range [29–31], these chemically deposited 2D materials usually suffer from poor carrier mobility and are therefore not suitable for studying phenomena such as cyclotron transitions [32].

The limiting factor in optically probing exfoliated 2D materials with high mobility in the THz range is the size in which the flakes can be extracted, which is typically in the range of $\approx 10 \mu m$, well below the THz wavelength on the order of ($\lambda \approx 1 mm$). Studies in the THz range of exfoliated flakes have therefore been restricted to the investigation of near field phenomena, such as on-chip THz

spectroscopy, or THz induced photocurrent experiments [33–35].

Here, we provide the first far field THz spectroscopy observation of Landau polaritons in monolayer graphene, in order to test the prediction of an emergent SRPT. We do this by employing an asymmetric solid immersion lens combined with a complementary meta-atom introduced in our previous works [36–38]. In this way, we can resolve the sub-wavelength ultrastrong coupling of a single complementary split ring resonator (cSRR) to an exfoliated high-mobility graphene flake in the THz regime. By electrostatic gating, we can tune the carrier density and through this the strength of the light-matter interaction [38, 39]. We compare the measured polariton asymptotes to those predicted within the Dicke and Hopfield models, shown for our system as a function of normalized carrier density and coupling strength in Figure 1a). We find excellent agreement with only the Hopfield model up to the measured density, indicated by the green dotted line in Figure 1a). This confirms the absence of SRPTs and provides an experimental answer to the long-standing theoretical debate about SRPTs in graphene polaritons [6, 7].

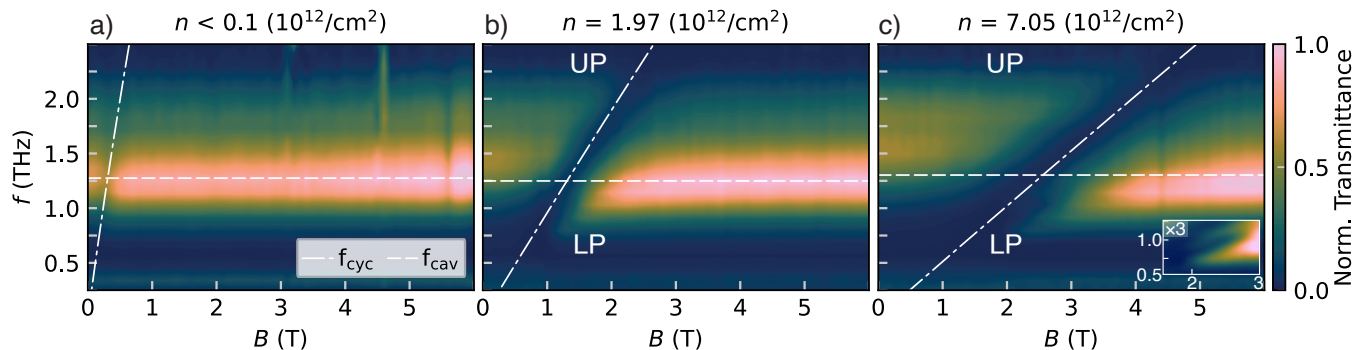


FIG. 2. **Tuning of cyclotron dispersion and light-matter coupling in monolayer graphene.** THz transmission spectroscopy as a function of the magnetic field with monolayer graphene biased at **a)** the CNP, **b)** an intermediate density $n = 1.97 \cdot 10^{12}/\text{cm}^2$, and **c)** $n = 7.05 \cdot 10^{12}/\text{cm}^2$, performed at a temperature of 3 K. The fitted cavity and cyclotron frequencies are indicated in each spectral map as white dashed and dashed-dotted lines, respectively. All data are referenced to the transmission spectrum of the bare SiO_2/Si substrate. The contrast of the color map is normalized to its maximum in each map separately. The inset of panel c) highlights a splitting of the LP branch by enhancing the contrast by a factor of 3.

FABRICATION AND MEASUREMENT METHODS

The considered sample consists of a fully encapsulated hBN - monolayer graphene - hBN stack, placed atop a thin chromium backgate (see Figure 1b), which is transmissive in the low-THz regime. The sample is equipped with three etch contacts [40] to monitor the source-drain current through the flake and to characterize the sample electrically. This is done with standard processes for lithography, dry-stacking and consequent reactive ion etching.

As presented in previous works [36–38], we can probe single cSRRs in the far field by placing a single resonator amid a large surface of gold, to suppress the transmission of THz radiation anywhere around the area of interest. This large ($d = 4$ mm) resonator surface is electrically insulated from the backgate and flake by atomic layer deposition of alumina. The deposited resonator is shown in Figure 1b. The cSRR dimensions are chosen to obtain a resonant frequency $f_{LC} = 1.27$ THz. This frequency lies in the middle of the setup’s probing bandwidth, and will be resonant with multiple intra-band graphene cyclotron transitions, depending on the carrier density n . A protective $2 \mu\text{m}$ thick buffer layer of BCB polymer is deposited over the entire resonator plane to maintain insulation of the different sample layers. The sample is then mounted in between the asymmetric solid immersion lenses (as shown in Figure 1c) and placed within a cryo-magnet, where we can reach a base temperature of 2.8 K, apply an out-of-plane magnetic field, and perform THz time-domain spectroscopy transmission measurements. The final sample layer structure is shown in Figure 1d, along with a finite element simulation of the field enhancement at resonance.

As a first step, the sample is electrically character-

ized with a charge neutrality point (CNP) measurement, and three point-contact quantum Hall measurements (see Supplementary Information). These measurements show a resistance peak at the CNP of $V_{CNP} = -0.46$ V, as well as clear Landau quantization as a function of the density for a fixed magnetic field.

RESULTS AND DISCUSSION

We perform THz time domain spectroscopy measurements for fixed densities as a function of the applied magnetic field B . In Figure 2 we present the spectra of exemplary measurements in the low, intermediate, and high density regimes. The remaining spectra can be found in the Supplementary Information.

At very low density close to the CNP, shown in Figure 2a, no avoided crossing is observable, with a very faint indication of cyclotron absorption at the anticrossing (resonant) magnetic field $B_{\times} = 0.5$ T. The measurement otherwise exhibits no dependence on the magnetic field. The sharp vertical features above $B = 3$ T in this spectrum, as well as in Figure 2c, arise from optical source instabilities and do not carry physical meaning. Additionally, consistent spectral features below 500 GHz show no dependence on n or B and will thus not be investigated further.

When the density is increased to $n = 1.97 \cdot 10^{12} \text{ cm}^{-2}$, shown in Figure 2b, a polariton splitting becomes clearly visible at $B_{\times} = 1.4$ T. The upper polariton (UP), visible at magnetic fields below $B = 2$ T, has blue-shifted in frequency away from the cavity frequency. Moreover, the lower polariton (LP) is visibly bending from as low as 750 GHz, up to the cavity frequency at high magnetic field.

Finally, in Figure 2c we present the spectral map at

the highest measured density of $n = 7.05 \times 10^{12} \text{ cm}^{-2}$. The anti-crossing field has shifted to $B_{\times} = 2.6 \text{ T}$, the UP is blue shifted even further, and the LP is asymptotically approaching a similar cavity frequency as in the previous cases.

To understand these spectra, we start with analyzing the change of the cyclotron frequency slope as a function of the density n . To this end, we need to look to the unique properties of graphene. By increasing n higher Landau Levels (LLs) N are populated, with transition energies quantified by the graphene LL energy $E_{N \rightarrow N+1} = \hbar\omega_{\text{cyc}} = \sqrt{2v_F^2 e B \hbar} (\sqrt{N+1} - \sqrt{N})$ which for high filling factors $\nu \gg 1$ simplifies in the following way [41]

$$\hbar\omega_{\text{cyc}} \simeq \sqrt{2v_F^2 e B \hbar} \frac{1}{2\sqrt{\nu}} = \hbar \frac{eBv_F^2}{E_F} = \hbar \frac{eB}{m^*}. \quad (1)$$

Herein, the Fermi velocity is assumed to be $v_F = 1 \times 10^6 \text{ m/s}$, and we have introduced the effective cyclotron mass of graphene $m^* = E_F/v_F^2$ that depends linearly on the Fermi energy E_F . Under the influence of strong magnetic fields, E_F is set by the LL energy E_N via the LL index. The filling factor ν is given in its usual form for massless Dirac fermions in graphene via $\nu = \frac{hn}{g_s e B}$, with the distinction of $g_s = 4$ taking into account the spin and valley degeneracies, leading to the relation $\nu = \text{sgn}(N)(|N| + \frac{1}{2})$, and $E_F = \sqrt{2e\hbar v_F^2(\nu + \frac{1}{2})}$ (details in the Supplementary Information). The quantization of the system into discrete Landau Levels is verified by the previously mentioned QH measurements. The change of ω_{cyc} with n is evidenced by the spectra presented in Figure 2, where the dashed-dotted white lines represent the fitted cyclotron dispersion ω_{cyc} . The effective cyclotron mass increases from $m^* \approx 0.01 \cdot m_e$ in Figure 2a, to $m^* \approx 0.03 \cdot m_e$ in Figure 2b, to the highest measured value of $m^* \approx 0.05 \cdot m_e$ in Figure 2c.

As the cavity frequency ω_{cav} is fixed by the resonator geometry, the magnetic field value at which ω_{cyc} anti-crosses with ω_{cav} will shift as the Fermi energy is changed. By rearranging equation 1 we can infer this magnetic field dependence on the filling factor:

$$B_{\times} = \frac{2\hbar\omega_{\text{cav}}^2}{ev_F^2} \nu. \quad (2)$$

This allows us to solve for the filling factor at B_{\times} , and obtain its square-root dependence on the carrier density: $\nu = \sqrt{n\pi v_F^2/g_s \omega_{\text{cav}}^2}$ (see Supplementary Information for details).

A novel emerging feature is highlighted in the inset of Figure 2c with increased contrast. The LP seems to be split into two distinct branches, discernible close to B_{\times} , before broadening and merging into one peak in the asymptotic limit. This splitting is consistently observed for high densities. Its evolution with the magnetic field is detailed in the Supplementary Information. A possible

explanation for this could be the non-coherent interaction of different plasmonic modes with the cavity at different momenta, leading to an overlap of two LPs asymptotically approaching the same cavity frequency with different coupling strengths. Alternatively, the splitting could arise from a degeneracy lifting of the carriers located in the K and K' valleys in the Brillouin zone of graphene. The relatively sharp linewidth of the feature hints at an interference of two excitations. Further discussion of the origin of this splitting is beyond the scope of this work.

In Figure 3a, we show the spectrum at maximum density together with the UP and LP branches for both the Hopfield and Dicke models in black solid and gray dashed lines, respectively. The black solid line clearly fits our data well, whereas the gray dashed line does not. This comparison suggests a Hopfield-like dispersion of our system and we have thus opted to perform systematic fits of our data with the Hopfield model. The spectra are first fitted with Lorentzian line shapes to extract the UP and LP peak positions, represented with white dots in Figure 3a. Then, the best fit is estimated for each measurement by way of root mean square (RMS) error minimization for different cavity frequencies, carrier densities, and coupling strengths. The fitting procedure for a selected spectrum, along with all optimally fitted dispersions can be viewed in the Supplementary Information. Doing so enables us to report the resulting normalized coupling ratio between the Rabi frequency and the cavity frequency $\eta = \Omega_R/\omega_{\text{cav}}$ and anticrossing positions B_{\times} as a function of carrier density irrespective of charge sign (see Figure 3b-c). We note that we observed no asymmetry in the light-matter coupling between electron and hole doping, see Supplementary Information for details. This is in agreement with expectations, as previous studies on Landau quantized graphene transport predict asymmetries well below our spectral resolution [42]. The densities extracted from the cyclotron slopes are in agreement with a plate capacitor model $n = \epsilon_0 \epsilon_{\text{hBN}} V/ed$, with the effective gate voltage $V = V_{\text{BG}} - V_{\text{CNP}}$, and $d = 25 \text{ nm}$ the hBN thickness (see Supplementary Information).

The Hopfield model for Landau polaritons has been previously derived for a wavelength-sized cavity whose field is given in terms of the (transverse) vector potential [6, 7]. In the setup considered here, graphene Landau excitations couple to the longitudinal near-field of the complementary split ring resonator described by the quasi-static scalar potential instead. To take this difference into account, we derive a Hopfield Hamiltonian that turns out to be equivalent to that in Ref. [7], starting from the quasi-static scalar potential of the longitudinal cavity field coupled to the charge density of the graphene Landau excitations in dipolar gauge. We find a P^2 term (that translates to a A^2 term via a Power-Zienau-Woolley transformation) by carefully tracing out all off-resonant field modes, while coupling of the field to interband transitions is shown to be suppressed in dipolar gauge, see

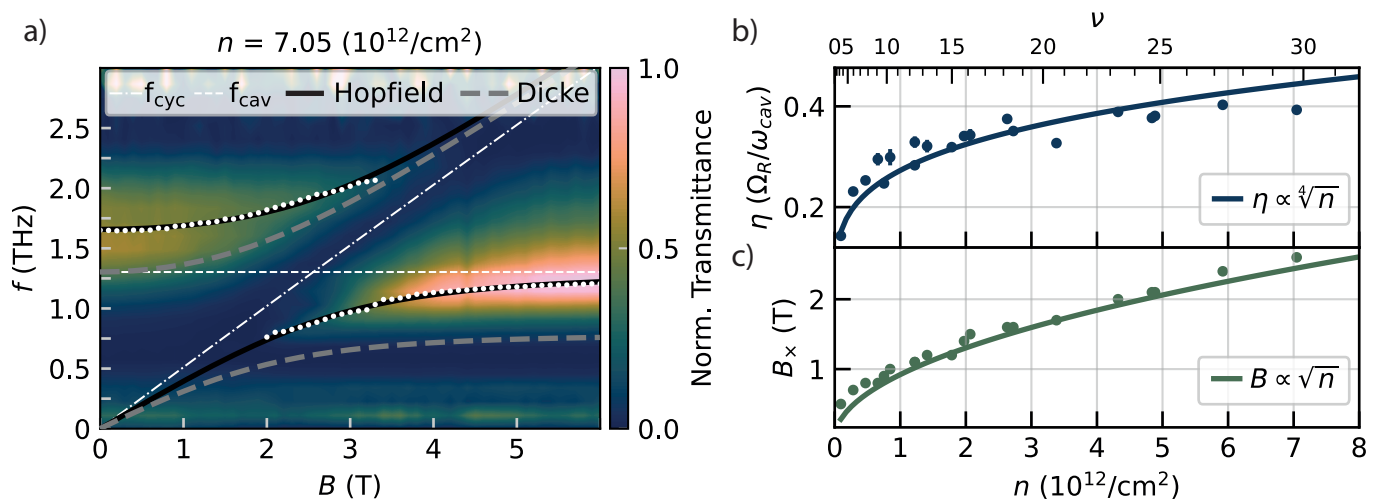


FIG. 3. **Density dependence of ultrastrong light-matter coupling in graphene.** **a)** Magnetic field-dependent spectral map at an electron density $n = 7.05 \times 10^{12}/\text{cm}^2$ overlaid with the Hopfield model fit (black line) to the fitted peak positions of the respective spectra (white dots). The gray dashed line shows the expected dispersion for UP and LP resulting from a Dicke Hamiltonian at the same cavity frequency and coupling strength. **b)** Coupling strengths η extracted from spectral measurements using the Hopfield-model fitting method as a function of density and filling factor, together with the analytical expression obtained from the quasi-static model. **c)** Extracted positions of the anti-crossing magnetic field, overlaid with the analytic expression given in Eq. 2.

Supplemental Material for details. This framework clarifies the presence of the A^2 term also for the near-field cavity employed here and allows to simulate the light-matter coupling constant via a finite-element simulation of the effective mode volume. The resulting computed normalized coupling ratios reported in Figure 3b show good agreement with our data, without any fitting parameters. We find enhanced coupling of the sub-wavelength resonator compared to a wavelength-sized Fabry-Perot cavity considered previously in Ref. [6].

The anticrossing magnetic field B_\times (Figure 3c), scales with the square root of the density. This is in precise agreement with the expression given in Equation 2, the analytical result of which is overlaid with a solid line for comparison. We can thereby confirm that the assumed Hopfield fits are consistent with our experimental findings, as well as general graphene cyclotron absorption properties.

In order to fully exclude the emergence of a Dicke SRPT in the measured density regime we can additionally study the trends of the UP and LP dispersions at minimal detuning ($B = 0$ T), at maximal detuning ($B = 6$ T) and at resonance ($B = B_\times$). We therefore report the fitted peak positions of UP and LP normalized to the respective fitted cavity frequencies in these distinct regimes in Figure 4a-c. All frequencies are plotted with error bars representing $\pm 3\sigma$ derived from the diagonal of the fit's covariance matrix. The shaded regions around the analytical curves indicate the spectral resolution of the measurements.

At $B = 0$ T (Figure 4a) the UP frequency blue-shifts

with increasing density, up to a factor of $1.2 \times f_{\text{cav}}$. This behavior is commensurate with a polariton gap opening as a consequence of diamagnetic contributions [7, 43]. These diamagnetic contributions $\Delta\omega$ (arising from the \vec{A}^2 -term) distinguish Hopfield and Dicke models, as they are neglected in a Dicke Hamiltonian [1, 2, 6, 7]. The blue-shift can be expressed via the coupling strength [43]

$$\frac{\Delta\omega}{\omega_{\text{cav}}} = \sqrt{4\eta^2 + 1} \quad (3)$$

and shows good agreement with the data, as can be seen from the solid red line in Figure 4a. In contrast, the UP mode of a Dicke model, which does not have any contributions from an \vec{A}^2 -term, stays fixed to the cavity frequency. This is shown by the gray dashed line in Figure 4a.

An even starker contrast is to be expected by the LP behavior at maximal detuning, as studied in Figure 4b. The hallmark of an SRPT is a continuous softening of the LP mode as the critical coupling is approached. While we observe a red-shift of $\approx 5\%$, this can be explained by the change in the cyclotron slope (B_\times) with the density. This effects a gradual change in the asymptotic behavior, which can also be calculated explicitly within a Hopfield formalism and has been overlaid as a solid blue line, again agreeing with the data. The softening of the LP mode in the Dicke model would induce a considerably stronger red-shift, as evidenced by the gray dashed curve shown in Figure 4b. In the case for the strongest expected coupling strength, the LP mode would spectrally converge to a frequency as low as $\approx 0.4 \times f_{\text{cav}}$.

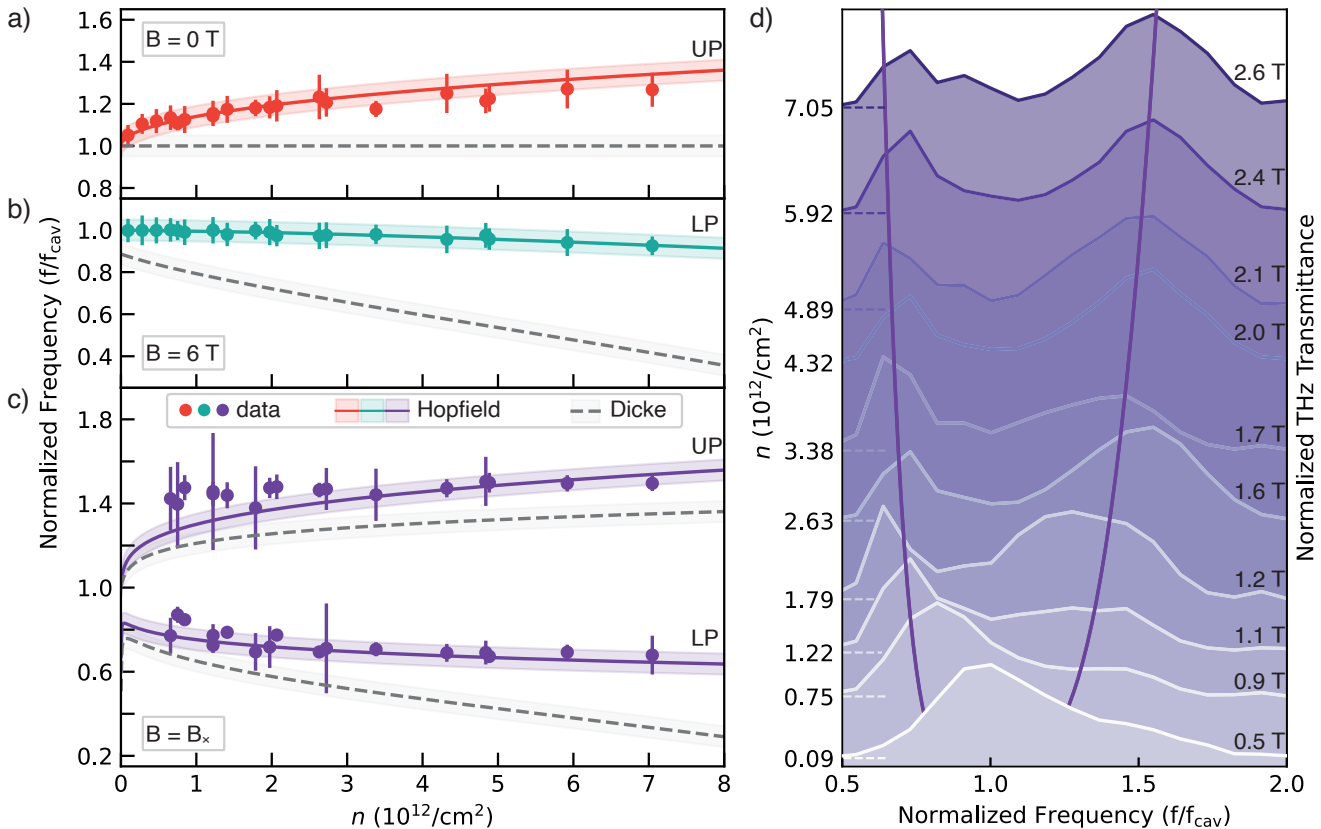


FIG. 4. **Absence of SRPT.** **a-c)** Normalized peak frequencies extracted from Lorentzian fits for a) the UP asymptote at $B = 0 \text{ T}$, b) the LP asymptote at $B = 6 \text{ T}$, and c) the UP and LP at the anticrossing magnetic field B_x for each respective density. Hopfield and Dicke model predictions are overlaid for each case in solid colored and dashed gray lines, respectively. The shaded area indicate the spectral resolution of the measurements. **d)** Measured THz transmittance spectra at B_x (varying with density, as indicated on the right). The y-offset corresponds to the density to show the evolution of the UP and LP splitting. Each spectrum is normalized separately. The purple lines correspond to the Hopfield model prediction (from panel c)).

At the respective resonance point B_x , we can study both UP and LP and directly observe the evolution of the branch splitting (Figure 4c). Once more the expectation for the Dicke branches is red-shifted considerably with regards to the measured data. The Hopfield branches adapted for the graphene system are overlaid in a solid purple line and again represent the data accurately. Selected corresponding spectra are shown in Figure 4d. This demonstrates the evolution of the polariton splitting as a function of density (coupling strength), represented by the y-axis offset of the normalized spectra, shown on the left side of the panel. The corresponding B_x are denoted on the right hand side. The purple line represents the identical Hopfield dispersion plotted in Figure 4c.

We therefore conclude that both polariton behaviors, measured over a wide range of densities and detunings (controlled via the magnetic field), are consistently described by a Hopfield Hamiltonian. This proves the emergence of diamagnetic contributions as argued in [7] and

also shown by our quasi-static model, and excludes the onset of an SRPT in graphene Landau polaritons. We note that the probed parameter space, fixed by the cavity mode ω_{cav} , is predicted to undergo the phase transition at the critical coupling strength $\eta_c = 0.52$ and critical density $n_c = 11.6 \times 10^{12} \text{ cm}^{-2}$, which is reachable in high quality heterostructures. While the measured range reported here lies below these critical values, the onset of this second order phase transition has been systematically disproved by investigating three distinct detuning regimes of the interaction. Moreover, finite temperature effects at the experimental temperature of 3 K do not appreciably alter the critical coupling condition, see Supplementary Information.

The phase boundaries are naturally affected by the tailored cavity frequency. For a cSRR resonant at $f_{\text{cav}} = 500 \text{ GHz}$, the critical density decreases to $n_c = 1.8 \times 10^{12} \text{ cm}^{-2}$. The normalized coupling strength however grows to $\eta_c \approx 80\%$ relative to the optical mode. A further drawback in this scenario would be the spa-

tial increase of the cSRR size to accommodate the longer wavelength, necessitating an even larger exfoliated material flake. Fabrication as well as graphene homogeneity pose limitations in this case, though not of fundamental nature. For a phase diagram showcasing the dependence of the SRPT onset as a function of density and cavity frequency, see Supplementary Information.

CONCLUSION

We have reported the first experimental observation of graphene Landau polaritons in the THz ultrastrong light-matter interaction regime. By placing an encapsulated monolayer of graphene underneath a single THz cSRR we were able to study the interaction via a far-field spectroscopy measurement. The system has been studied at different densities, which enabled us to verify the Hopfield-like nature of the interaction in the accessed range. In doing so, we can confirm the importance of the diamagnetic contribution to the Hamiltonian and offer first experimental insights into the many-body response of graphene Landau polaritons at low energy scales.

While inter-level Landau transitions are not targeted within the studied frequency range, it becomes apparent that the overall f-sum rule for the allowed dipolar transitions of carriers in graphene governs the system's electronic response. The experiment therefore validates fundamental principles such as gauge invariance, charge-current conservation, and the conservation of the total spectral weight of the allowed transitions. Importantly, our experimental results clearly contradict the appearance of a SRPT in the graphene Landau polariton system. The emerging LP splitting at high carrier densities remains an intriguing feature to be studied in different sample geometries, to discern its plasmonic [35] or intrinsic nature.

The presented results, together with those presented in [37], open the path for spectroscopy experiments in the terahertz range with a multitude of different exfoliated van der Waals materials. This could provide insights into the low-energy physics of such systems, a field that has been limited to transient field studies and electronic response due to the inherent sub-wavelength nature of these materials in the THz range.

ACKNOWLEDGEMENTS

The authors thank M. Barra Burillo for help in the initial part of the project. F.H. and T.F.N. thank A. İmamoğlu for his continuous support. E.J. thanks A. İmamoğlu for the use of his facilities. We acknowledge the cleanroom facility FIRST at ETH Zürich. E.J. and F.H. acknowledge discussions on sample fabrication with the Ensslin group at ETH.

FUNDING

E.J., L.H., L.G., J.F., and G.S. acknowledge funding by the Swiss National Science Foundation (SNF) (Grant numbers 10000397 and 200020-207795). F.H. acknowledges support from the Swiss National Science Foundation (SNF) (Grant number 200020 207520). M.J. acknowledges funding by the US Department of Energy (Grant number DE-SC0016925). T.F.N. acknowledges funding from the ETH postdoctoral fellowship program. F.L. was supported by the Quantum Center Research Fellowship and the Dr Alfred and Flora Spälti Fonds.

-
- [1] K. Hepp and E. H. Lieb, On the superradiant phase transition for molecules in a quantized radiation field: the Dicke maser model, *Annals of Physics* **76**, 360 (1973).
 - [2] Y. K. Wang and F. T. Hioe, Phase Transition in the Dicke Model of Superradiance, *Physical Review A* **7**, 831 (1973).
 - [3] K. Rzażewski, K. Wódkiewicz, and W. Żakowicz, Phase Transitions, Two-Level Atoms, and the $\{A\}^2$ Term, *Physical Review Letters* **35**, 432 (1975).
 - [4] J. M. Knight, Y. Aharonov, and G. T. C. Hsieh, Are super-radiant phase transitions possible?, *Physical Review A* **17**, 1454 (1978).
 - [5] K. Gawędzki and K. Rzażewski, No-go theorem for the superradiant phase transition without dipole approximation, *Physical Review A* **23**, 2134 (1981), publisher: American Physical Society.
 - [6] D. Hagenmüller and C. Ciuti, Cavity QED of the Graphene Cyclotron Transition, *Physical Review Letters* **109**, 267403 (2012).
 - [7] L. Chirolli, M. Polini, V. Giovannetti, and A. H. MacDonald, Drude Weight, Cyclotron Resonance, and the Dicke Model of Graphene Cavity QED, *Physical Review Letters* **109**, 267404 (2012).
 - [8] R. H. Dicke, Coherence in Spontaneous Radiation Processes, *Physical Review* **93**, 99 (1954), aDS Bibcode: 1954PhRv...93...99D.
 - [9] M. Gross and S. Haroche, Superradiance: An essay on the theory of collective spontaneous emission, *Physics Reports* **93**, 301 (1982).
 - [10] P. Kirton, M. M. Roses, J. Keeling, and E. G. D. Torre, Introduction to the Dicke model: from equilibrium to nonequilibrium, and vice versa, *Advanced Quantum Technologies* **2**, 1800043 (2019), arXiv:1805.09828 [quant-ph].
 - [11] F. Schlawin, D. M. Kennes, and M. A. Sentef, Cavity quantum materials, *Applied Physics Reviews* **9**, 011312 (2022).
 - [12] A. T. Black, H. W. Chan, and V. Vuletić, Observation of Collective Friction Forces due to Spatial Self-Organization of Atoms: From Rayleigh to Bragg Scattering, *Physical Review Letters* **91**, 203001 (2003).
 - [13] K. Baumann, C. Guerlin, F. Brennecke, and T. Esslinger, Dicke quantum phase transition with a superfluid gas in an optical cavity, *Nature* **464**, 1301 (2010).

- [14] Z. Zhiqiang, C. H. Lee, R. Kumar, K. J. Arnold, S. J. Masson, A. S. Parkins, and M. D. Barrett, Nonequilibrium phase transition in a spin-1 Dicke model, *Optica* **4**, 424 (2017).
- [15] K. Cong, Q. Zhang, Y. Wang, G. T. Noe, A. Belyanin, and J. Kono, Dicke superradiance in solids (invited), *J. Opt. Soc. Am. B* **33**, C80 (2016).
- [16] D. Kim, S. Dasgupta, X. Ma, J.-M. Park, H.-T. Wei, X. Li, L. Luo, J. Doumani, W. Yang, D. Cheng, R. H. J. Kim, H. O. Everitt, S. Kimura, H. Nojiri, J. Wang, S. Cao, M. Bamba, K. R. A. Hazzard, and J. Kono, Observation of the magnonic dicke superradiant phase transition, *Science Advances* **11**, eadt1691 (2025), <https://www.science.org/doi/pdf/10.1126/sciadv.adt1691>.
- [17] P. Nataf and C. Ciuti, No-go theorem for superradiant quantum phase transitions in cavity QED and counterexample in circuit QED, *Nature Communications* **1**, 72 (2010), number: 1.
- [18] C. Schäfer, M. Ruggenthaler, V. Rokaj, and A. Rubio, Relevance of the Quadratic Diamagnetic and Self-Polarization Terms in Cavity Quantum Electrodynamics, *ACS Photonics* **7**, 975 (2020).
- [19] V. Rokaj, M. Ruggenthaler, F. G. Eich, and A. Rubio, Free electron gas in cavity quantum electrodynamics, *Physical Review Research* **4**, 013012 (2022).
- [20] J. J. Hopfield, Theory of the Contribution of Excitons to the Complex Dielectric Constant of Crystals, *Physical Review* **112**, 1555 (1958).
- [21] A. F. Kockum, Ultrastrong coupling between light and matter | *Nature Reviews Physics*.
- [22] P. Forn-Díaz, L. Lamata, E. Rico, J. Kono, and E. Solano, Ultrastrong coupling regimes of light-matter interaction, *Reviews of Modern Physics* **91**, 025005 (2019).
- [23] J. Keller, G. Scalari, F. Appugliese, S. Rajabali, M. Beck, J. Haase, C. A. Lehner, W. Wegscheider, M. Failla, M. Myronov, D. R. Leadley, J. Lloyd-Hughes, P. Nataf, and J. Faist, Landau polaritons in highly nonparabolic two-dimensional gases in the ultrastrong coupling regime, *Physical Review B* **101**, 075301 (2020).
- [24] A. Vukics, T. Griebner, and P. Domokos, Elimination of the λ -Square Problem from Cavity QED, *Physical Review Letters* **112**, 073601 (2014).
- [25] B. Gulácsi and B. Dóra, From Floquet to Dicke: Quantum Spin Hall Insulator Interacting with Quantum Light, *Physical Review Letters* **115**, 160402 (2015).
- [26] T. Jaako, Z.-L. Xiang, J. J. Garcia-Ripoll, and P. Rabl, Ultrastrong-coupling phenomena beyond the Dicke model, *Physical Review A* **94**, 033850 (2016).
- [27] G. M. Andolina, F. M. D. Pellegrino, V. Giovannetti, A. H. MacDonald, and M. Polini, Cavity quantum electrodynamics of strongly correlated electron systems: A no-go theorem for photon condensation, *Physical Review B* **100**, 121109 (2019).
- [28] A. Stokes and A. Nazir, Uniqueness of the Phase Transition in Many-Dipole Cavity Quantum Electrodynamical Systems, *Physical Review Letters* **125**, 143603 (2020).
- [29] F. Valmorra, G. Scalari, C. Maissen, W. Fu, C. Schönenberger, J. W. Choi, H. G. Park, M. Beck, and J. Faist, Low-Bias Active Control of Terahertz Waves by Coupling Large-Area CVD Graphene to a Terahertz Metamaterial, *Nano Letters* **13**, 3193 (2013).
- [30] L. Ren, Q. Zhang, J. Yao, Z. Sun, R. Kaneko, Z. Yan, S. Nanot, Z. Jin, I. Kawayama, M. Tonouchi, J. M. Tour, and J. Kono, Terahertz and Infrared Spectroscopy of Gated Large-Area Graphene, *Nano Letters* **12**, 3711 (2012).
- [31] S. Zanotto, C. Lange, T. Maag, A. Pitanti, V. Miseikis, C. Coletti, R. Degl'Innocenti, L. Baldacci, R. Huber, and A. Tredicucci, Magneto-optic transmittance modulation observed in a hybrid graphene-Åsplit ring resonator terahertz metasurface, *Applied Physics Letters* **107**, 121104 (2015).
- [32] D. De Fazio, D. G. Purdie, A. K. Ott, P. Braeuninger-Weimer, T. Khodkov, S. Goossens, T. Taniguchi, K. Watanabe, P. Livreri, F. H. L. Koppens, S. Hofmann, I. Goykhman, A. C. Ferrari, and A. Lombardo, High-Mobility, Wet-Transferred Graphene Grown by Chemical Vapor Deposition, *ACS Nano* **13**, 8926 (2019), publisher: American Chemical Society.
- [33] T. Han, J. Yang, Q. Zhang, L. Wang, K. Watanabe, T. Taniguchi, P. L. McEuen, and L. Ju, Accurate measurement of the gap of Graphene/ h -BN moiré superlattice through photocurrent spectroscopy, *Phys. Rev. Lett.* **126**, 146402 (2021).
- [34] W. Zhao, S. Wang, S. Chen, Z. Zhang, K. Watanabe, T. Taniguchi, A. Zettl, and F. Wang, Observation of hydrodynamic plasmons and energy waves in graphene, *Nature* **614**, 688 (2023).
- [35] G. Kipp, H. M. Bretscher, B. Schulte, D. Herrmann, K. Kussyak, M. W. Day, S. Kesavan, T. Matsuyama, X. Li, S. M. Langner, J. Hagelstein, F. Sturm, A. M. Potts, C. J. Eckhardt, Y. Huang, K. Watanabe, T. Taniguchi, A. Rubio, D. M. Kennes, M. A. Sentef, E. Baudin, G. Meier, M. H. Michael, and J. W. McIver, Cavity electrodynamics of van der Waals heterostructures, *Nature Physics* **21**, 1926 (2025).
- [36] S. Rajabali, S. Markmann, E. Jöchl, M. Beck, C. A. Lehner, W. Wegscheider, J. Faist, and G. Scalari, An ultrastrongly coupled single terahertz meta-atom, *Nature Communications* **13**, 2528 (2022), number: 1.
- [37] F. Helmrich, H. S. Adlong, I. Khanonkin, M. Kroner, G. Scalari, J. Faist, A. Imamoglu, and T. F. Nova, Cavity-Driven Attractive Interactions in Quantum Materials, *Nature* 10.1038/s41586-026-10609-1 (2026).
- [38] E. Jöchl, A.-L. Vieli, L. Hale, F. Helmrich, D. Turan, M. Jarrahi, M. Beck, J. Faist, and G. Scalari, Gate-Tunable Single Terahertz Meta-Atom Ultrastrong Light-Matter Coupling, *ACS Photonics* **13**, 1122 (2026).
- [39] M. Malerba, S. Pirota, G. Aubin, L. Lucia, M. Jeannin, J.-M. Manceau, A. Bousseksou, Q. Lin, J.-F. Lampin, E. Peytavit, S. Barbieri, L. H. Li, A. G. Davies, E. H. Linfield, and R. Colombelli, Ultrafast (≈ 10 ghz) mid-ir modulator based on ultrafast electrical switching of the light-matter coupling, *Applied Physics Letters* **125**, 041101 (2024).
- [40] L. Wang, I. Meric, P. Y. Huang, Q. Gao, Y. Gao, H. Tran, T. Taniguchi, K. Watanabe, L. M. Campos, D. A. Muller, J. Guo, P. Kim, J. Hone, K. L. Shepard, and C. R. Dean, One-Dimensional Electrical Contact to a Two-Dimensional Material, *Science* **342**, 614 (2013).
- [41] B. Benhamou-Bui, C. Consejo, S. S. Krishnopenko, S. Ruffenach, C. Bray, J. Torres, J. Dzian, F. Le Mardelé, A. Pagot, X. Baudry, S. V. Morozov, N. N. Mikhailov, S. A. Dvoretzkii, B. Jouault, P. Ballet, M. Orlita, C. Ciuti, and F. Teppe, Nonlinear terahertz electroluminescence from dirac-landau polaritons, *Phys. Rev. Lett.* **136**, 096902 (2026).

- [42] Y. Zhang, Y.-W. Tan, H. L. Stormer, and P. Kim, Experimental observation of the quantum Hall effect and Berry's phase in graphene, *Nature* **438**, 201 (2005), number: 7065.
- [43] C. Maissen, G. Scalari, F. Valmorra, M. Beck, J. Faist, S. Cibella, R. Leoni, C. Reichl, C. Charpentier, and W. Wegscheider, Ultrastrong coupling in the near field of complementary split-ring resonators, *Physical Review B* **90**, 205309 (2014).